OMASTAR Optimal Magnetic Actuation System Arrangement

Veerash Palanichamy, Hussein Saad, Matthew Giamou, Onaizah Onaizah

***Abstract*— Microrobots and other miniature robots are able to access millimeter-sized spaces and thus have the potential to solve many challenging problems in healthcare. However, clinical adoption of these robots is rare as these systems are often difficult to scale up. One such issue arises from the actuation systems used to remotely control magnetic microrobots, which tend to be bulky and obstruct the surgeons' workspaces. They also do not guarantee wide ranges of magnetic fields and forces in a large patient-sized workspace. In this paper, we present the design of a permanent magnet-based actuation system that fits within a 40 cm cube of space under an operating table. We also formulate a new set function maximization-based approach for efficiently designing E-optimal magnet arrangements with off-the-shelf convex solvers. Our optimization method is evaluated with synthetic data and a proof-of-concept of the system is simulated.**

***Index Terms*– microrobots, magnetic actuation, patient-size workspace, optimization, medical applications.**

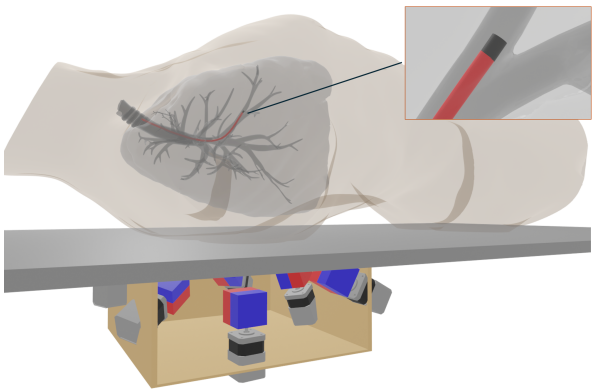

Fig. 1: Render of an under-the-table actuation system being used to navigate a catheter with a magnetic tip inside the lungs [15].

I. Introduction

Microrobotics is a popular area of research because of its potential applications in medical diagnosis and treatment [1]. However, the transition from research to clinical use has been slow and filled with barriers [2]. One of the biggest challenges for clinical use is building systems for remote control of these robots within the human body [3], [4]. Remote actuation of microrobots can be achieved through a number of different techniques; magnetic fields are commonly used as they can penetrate the human body and have a high level of controllability [5]. Magnetic fields can be generated through either electromagnetic coils or external permanent magnets. Although various designs of magnetic actuation systems have been proposed, most of them scale poorly for large patient-sized workspaces in a clinical scenario. An ideal magnetic actuation system should use minimal space inside the operating room, allowing the surgeon to work while generating the required fields and forces across a large workspace.

Positioning the magnetic actuation system under the operating table is one way of tackling space constraints while keeping it close to the workspace. One recently proposed design used electromagnets under the operating table to actuate magnetic micro-surgical tools in the brain [6]. Another actuation system [7] used a set of coils under the table and another set above the patient. Many magnetic actuation systems use electromagnetic coils [8], [9]; however, these systems are difficult to scale up, as the maximum magnetic forces are highly dependent on coil parameters and high currents. Increasing coil sizes takes up more space, while higher currents consume more energy and often lead to systems that require a cooling system to manage increased heat generation [10].

Contrastingly, permanent magnets are more energy-dense and therefore capable of producing higher fields and forces with no significant heat generation. An existing clinical platform (the *Stereotaxi Niobe* system) [11] has two permanent magnets distributed on the opposite sides of the bed. This system is used to navigate catheters in the lungs. Other platforms have been developed for similar purposes, such as the dEPM [12], which uses two large cylindrical permanent magnets mounted on two KUKA robot arms. These systems still pose a challenge in an operating room as they require complex motorized actuation which affects response time [13], take up space in the room, and are also cost prohibitive, with each robot arm retailing for upwards of $100,000.

This work proposes an actuation system that minimizes clutter by using permanent magnets that are completely under the operating table. Based on the work of Ryan & Diller [14], the proposed system uses the rotation of optimally placed magnets to generate the required field and forces at a target location to enable control over 5 degrees of freedom (DOF). Each magnet is rotated using a simple DC stepper motor. The magnets are all located within a small box as shown in Fig. 1 that can be translated in the x-y plane to any position under the table based on the required application of the system.

As the placement of the magnets dictates the controllability of our system, this work introduces the *Optimal Magnetic Actuation SysTem ARrangement* (OMASTAR) method for computing magnet poses in our design. OMASTAR is based on an information-theoretic methodology for finding the

All authors are with the Department of Computing and Software, McMaster University, Hamilton, ON, CA [palanicv, saadh, giamoum, onaizaho]@mcmaster.ca

We acknowledge support from the Natural Sciences and Engineering Research Council of Canada (NSERC) Discovery Grant and the Canada Foundation for Innovation.

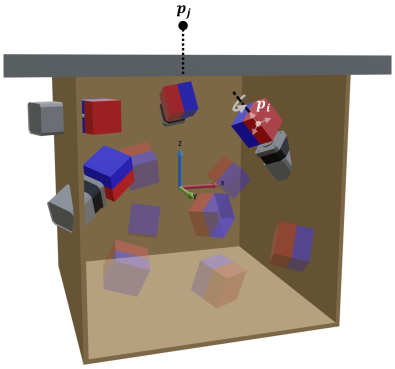

Fig. 2: Schematic image showing $K = 4$ magnets chosen from $M = 11$. $\boldsymbol{p}_i$ represents the center of the actuator magnet and $\boldsymbol{p}_j$ the target location

optimal arrangement of sensors for robot localization and mapping [16]. This approach uses set function optimization to pick a subset of optimal magnet positions and orientations from a large randomized sample rather than directly optimizing non-linear cost functions that arise from magnetostatic equations. Our implementation is freely available online.[1]

The remainder of the paper is structured as follows. Section II describes the basic design and construction of the system. Section III provides a novel optimization method to find optimal placements of magnets to achieve the best fields and forces at our target location. Section IV evaluates our optimization method. Lastly, our design is used for actuation of a microrobot in a simulation environment.

II. Design & Construction

The actuation system consists of K magnets located within a 40 cm cubic region under the operating table as shown in Fig. 2. Each of these magnets is mounted on a stepper motor, enabling it to rotate around a single axis. Varying angular positions of the magnet produce different fields and field gradients at the target location $\boldsymbol{p}_j$. The magnetic field at $\boldsymbol{p}_j$ due to a magnetic dipole $\boldsymbol{m}_i$ located at $\boldsymbol{p}_i$ is

$$\boldsymbol{B}(\boldsymbol{r}_{ij}) = \left(\frac{\mu_0}{4\pi ||\boldsymbol{r}_{ij}||^3} (3\hat{\boldsymbol{r}}_{ij}\hat{\boldsymbol{r}}_{ij}^{\intercal} - \mathbb{I}_3) \right) \boldsymbol{m}_i, \tag{1}$$

where $\boldsymbol{r}_{ij} = \boldsymbol{p}_j - \boldsymbol{p}_i$. The magnetic field at $\boldsymbol{p}_j$ from K magnets is therefore

$$\boldsymbol{B}(\boldsymbol{p}_j) = \sum_{i=1}^{K} \boldsymbol{B}(\boldsymbol{r}_{ij}). \tag{2}$$

When subjected to a magnetic field, a microrobot with magnetic moment $\boldsymbol{m}_j$ will rotate to align with the field due to a torque

$$\boldsymbol{\tau}(\boldsymbol{p}_j) = \boldsymbol{m}_j \times \boldsymbol{B}(\boldsymbol{p}_j). \tag{3}$$

Similarly, the force exerted on a target with magnetic moment $\boldsymbol{m}_j$ at $\boldsymbol{p}_j$ is:

$$\begin{aligned} \boldsymbol{F}(\boldsymbol{p}_j, \boldsymbol{m}_j) &= (\boldsymbol{m}_j \cdot \nabla)\boldsymbol{B}(\boldsymbol{p}_j) \\ &= \sum_{i=1}^{K} \Bigg[\frac{3\mu_0 \|\boldsymbol{m}_i\|}{4\pi \|\boldsymbol{r}_{ij}\|^4} \big(\hat{\boldsymbol{m}}_i \hat{\boldsymbol{r}}_{ij}^{\top} + \hat{\boldsymbol{r}}_{ij} \hat{\boldsymbol{m}}_i^{\top} \\ &\quad - [5\hat{\boldsymbol{r}}_{ij}\hat{\boldsymbol{r}}_{ij}^{\top} - I](\hat{\boldsymbol{m}}_i \cdot \hat{\boldsymbol{r}}_{ij}) \big) \Bigg] \boldsymbol{m}_j. \end{aligned} \tag{4}$$

The magnetic dipole of the ith permanent magnet is invariant to rotations about its axis $\boldsymbol{m}_i$, meaning the feasible set of each design variable is the product manifold

$$\mathcal{M} \triangleq \mathbb{R}^3 \times S^2 \times \mathbb{R}_+, \tag{5}$$

where the three terms of the product are the magnet's position, dipole direction, and magnetization. As the magnet rotates, the direction of the magnetic moment will change. In our design, the magnet rotates about its local z-axis with the magnetization vector in the x-y plane. The unit vector of the magnetic moment for a magnet rotated by θ_i relative to its local coordinate system is

$$\hat{\boldsymbol{m}}_i' = \begin{bmatrix} \cos(\theta_i) & \sin(\theta_i) & 0 \end{bmatrix}^{\top}. \tag{6}$$

Therefore, the unit vector of the magnetic moment in the global coordinate system is

$$\hat{\boldsymbol{m}}_i = \boldsymbol{R}_i \cdot \hat{\boldsymbol{m}}_i', \tag{7}$$

where $\boldsymbol{R}_i$ is the rotation matrix that transforms the local orientation to the global one.

A range of magnetic torques and forces can be achieved by varying the magnets' angular position. To achieve 5-DOF control, a nonlinear least squares formulation is used for the inverse kinematics [14]:

$$\min_{\boldsymbol{\theta} \in S^n} c_B \|\boldsymbol{B}(\boldsymbol{\theta}) - \boldsymbol{B}_0\|^2 + (1 - c_B)\|\boldsymbol{F}(\boldsymbol{\theta}) - \boldsymbol{F}_0\|^2, \tag{8}$$

where $\boldsymbol{\theta}_i \in S^1$ parameterizes the revolute configuration of the ith permanent magnet, and $\boldsymbol{B}_0$ and $\boldsymbol{F}_0$ are the desired field and force. Using this definition of inverse kinematics, we can reverse-engineer a definition for the "magnetic forward kinematics":

$$f(\boldsymbol{\theta}) \triangleq \begin{bmatrix} \boldsymbol{B}(\boldsymbol{\theta}) \\ \boldsymbol{F}(\boldsymbol{\theta}) \end{bmatrix}. \tag{9}$$

III. Magnet Optimization

Our method aims to find positions and orientations of K magnets that achieve diverse fields and forces over a set of discretized motor angles Θ by maximizing manipulability. Our problem formulation leads to a nonlinear integer program with a natural convex relaxation which can be efficiently solved for high-quality approximate solutions.

A. Manipulability

The traditional definition of manipulability for a robot with forward kinematics $\boldsymbol{x} = f(\boldsymbol{\theta})$ is

$$\mu(\boldsymbol{\theta}) \triangleq \prod_{i=1}^{n} \sigma_i \propto \sqrt{\det\left(\boldsymbol{J}(\boldsymbol{\theta})\, \boldsymbol{J}(\boldsymbol{\theta})^{\top} \right)}, \tag{10}$$

[1] https://github.com/HeartLab-McMaster/MagnetOptimization

where $\boldsymbol{J}$ is the Jacobian of f and σ_i is its ith singular value [17]. We therefore define the manipulability of a magnetic actuation system as Equation (10), where $\boldsymbol{J}$ is the Jacobian of the magnetic forward kinematics in Equation (9). Manipulability is proportional to the volume of the ellipsoid described by $\boldsymbol{J}(\boldsymbol{\theta})\ \boldsymbol{J}(\boldsymbol{\theta})^\top$. In this work, we maximize the shortest principal axis of the manipulability ellipsoid, which is equivalent to

$$f_E \triangleq \lambda_{\min}(\boldsymbol{J}(\boldsymbol{\theta})\ \boldsymbol{J}(\boldsymbol{\theta})^\top), \tag{11}$$

leading to an approach analogous to E-optimal Bayesian experimental design [18]. Our experimental results in Section IV confirm that configurations maximizing this objective provide a variety of field and force outputs as desired.

B. Constraints

Rather than optimize a nonlinear objective function like Equation (10) over the nonconvex continuous domain $\mathcal{M}^N$, we discretize the problem by specifying $M \gg K$ elements of $\mathcal{M}$ as candidate poses for the design of a magnetic actuation system. Our objective function therefore requires a parametrization of $\boldsymbol{J}(\boldsymbol{\theta})$ in terms of the selected magnet poses. As such, we introduce the variable

$$\boldsymbol{X} \in \{0,1\}^{K\times M}, \tag{12}$$

whose entries encode whether the ith of K selected magnets should be placed in the jth of the M candidate poses. Our decision variable $\boldsymbol{X}$ is subject to

$$\begin{aligned} \boldsymbol{X}\mathbf{1}_M &= \mathbf{1}_K, \\ \mathbf{1}_K^\top \boldsymbol{X} &\leq \mathbf{1}_M^\top, \end{aligned} \tag{13}$$

the first of which ensures that K magnets are placed, and the second of which permits at most one magnet in each of the M candidate poses. We have used $\mathbf{1}_N \in \mathbb{R}^N$ to denote a column vector of ones length N.

Some of the M candidate magnet poses in $\mathcal{M}$ may physically overlap for one or more configurations $\boldsymbol{\theta}$. Therefore, for each set of indices $\mathcal{J} \subset [M]$ that leads to overlapping magnets, we introduce the *mutual exclusivity* constraint

$$\sum_{i=1}^{K}\sum_{j\in\mathcal{J}} \boldsymbol{X}_{i,j} \leq 1, \tag{14}$$

which eliminates unrealizable designs.

C. OMASTAR

Our manipulability score as a function of $\boldsymbol{X}$ is

$$f_\mu(\boldsymbol{X}) \triangleq \min_{\boldsymbol{\theta}\in\Theta} \lambda_{\min}\left(\sum_{i=1}^{K}\sum_{j=1}^{M} \boldsymbol{X}_{i,j}\boldsymbol{A}_{\boldsymbol{\theta}_i,j}\right), \tag{15}$$

where

$$\boldsymbol{A}_{\boldsymbol{\theta}_i,j} \triangleq \boldsymbol{J}_j(\boldsymbol{\theta}_i)\boldsymbol{J}_j(\boldsymbol{\theta}_i)^\top \in \mathbb{S}^6, \tag{16}$$

and $\boldsymbol{J}_j(\boldsymbol{\theta}_i) \in \mathbb{R}^6$ is the Jacobian of the magnetic force and field induced by the magnet in pose $j \in [M]$ at angle $\boldsymbol{\theta}_i$. The full magnet placement problem is therefore:

Problem 1 (Magnet Placement):

$$\begin{aligned} \max_{\boldsymbol{X}\in\{0,1\}^{K\times M}}\ & f_\mu(\boldsymbol{X}) \\ \text{s.t. } & \boldsymbol{X}\mathbf{1}_M = \mathbf{1}_K, \\ & \mathbf{1}_K^\top \boldsymbol{X} \leq \mathbf{1}_M^\top. \end{aligned} \tag{17}$$

D. Convex Relaxations

Problem 1 is a nonlinear integer program and therefore NP-hard in general [19]. To solve it efficiently, we relax the nonconvex constraints on each boolean element of $\boldsymbol{X}$ by allowing it to take on any value in $[0,1]$, leading to the following convex program:

Problem 2 (Convex Relaxation):

$$\begin{aligned} \max_{t,X}\ & t \\ \text{s.t. } & \boldsymbol{X} \in [0,1]^{K\times M}, \\ & \boldsymbol{X}\mathbf{1}_M = \mathbf{1}_K, \\ & \boldsymbol{X}^\top\mathbf{1}_K \leq \mathbf{1}_M, \\ & t \leq \lambda_{\min}\left(\sum_{i=1}^{K}\sum_{j=1}^{M} \boldsymbol{X}_{i,j}\boldsymbol{A}_{\boldsymbol{\theta}_i,j}\right)\ \forall \boldsymbol{\theta} \in \Theta. \end{aligned} \tag{18}$$

Note that we have replaced the nested minimization of f_μ with an equivalent constrained variable $t \in \mathbb{R}$ [20].

After solving Problem 2 for maximizer $\boldsymbol{X}^\star \in [0,1]^{K\times M}$, the elements of $\boldsymbol{X}^\star$ must be rounded to integer values to choose the optimal K magnet poses. For this work, we use a simple rounding method where the columns are summed to form a vector of M values, and the indices of the K largest elements are chosen as the solution, breaking ties at random as in [21].

IV. Evaluation

A. Setup used for optimization

The actuator magnets used are 5 cm cubes, each with a magnetic moment $\|m_i\| = 136.66$ Am^2 (based on the magnetization of an N42 rare-earth magnet). These magnets are positioned within a 40 cm cube. The target location where the forces and fields are calculated ($\boldsymbol{p}_j$) is 15 cm away from the top of the cube. The size limitation for the magnet location was specifically chosen to ensure the final system could fit under an operating table while using up minimal space. The magnets must also maintain at least a 7.5 cm separation distance to minimize the magnetic interaction forces and torques.

The target magnet used in the force calculation is a 3 mm magnet with a magnetic moment $\|m_j\| = 28$ mA·m^2 placed at the target location in a fixed orientation for all optimization. Although the optimization problem can be reframed to work with field gradients instead of forces to eliminate the need for a target magnetic dipole, the optimal results were very similar during initial testing, thus all other evaluation in this paper was done using forces. This helps reduce the variable size which makes the optimization more efficient.

The result from our optimizer is a set of K magnet poses. To evaluate these solutions, we can measure the minimum

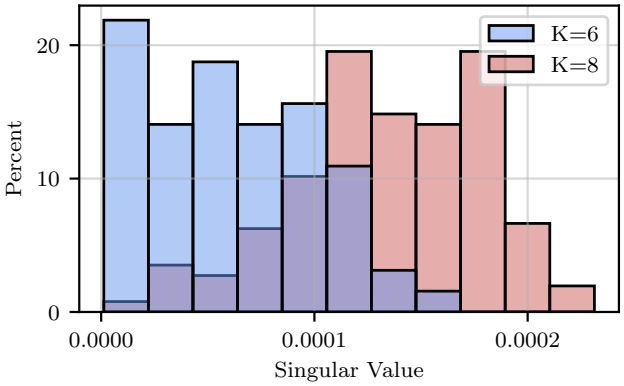

Fig. 3: Minimum singular value ($\sigma_{\min}$) distributions over all angles for 8-magnet vs 6-magnet configuration

singular value $\sigma_{\min}$ of the concatenated Jacobian over the set of sampled angles Θ.

$$\sigma_{\min}(\boldsymbol{\theta}) = \sigma_n\left([J_0(\boldsymbol{\theta}) \cdots J_{K-1}(\boldsymbol{\theta})]\right) \tag{19}$$

An increasing value of $\sigma_{\min}$ means our system is more controllable thus achieving a wide variety of fields and forces and eliminating any singularity.

B. Choosing M and K

Although 5-DOF control is possible using 6 magnets [22] for specific microrobot orientations, the final simulated system and most of the evaluation in this work was done using an 8-magnet setup. As shown in Fig. 3, the configuration with 8 magnets demonstrates significantly better controllability compared to the 6-magnet configuration. More magnets allow for a larger net magnetic moment and offer more configurations of magnet rotations to generate varying fields and forces.

To ensure our solution is closer to the optimum, the size of M is much larger than K. This enables sampling of a large number of poses to find the best combination. Fig. 4 shows the effect of increasing M on the distribution of $\sigma_{\min}$ suggesting that the minimum singular values over all angles improve as M increases. The drawbacks of a larger M are an increase in problem space and optimization time. However, since the optimization has to be completed only once to compute the best configuration, computation time is not a significant barrier.

C. Comparison of optimization result

For small M and K, it is possible to compare the performance of the optimizer to brute force solutions. The brute force approach is to try all possible combinations of K magnets from M to find one that will result in the largest minimum value of the $\sigma_{\min}$ over all angles.

For 100 trials, the minimum $\sigma_{\min}$ over all angles was calculated for a problem setup of $M = 10, K = 6$. The distribution statistics are reported in Table I. As expected, the relaxed solution outperforms other approaches as it partially weighs each magnet's contribution, but it is not a physically

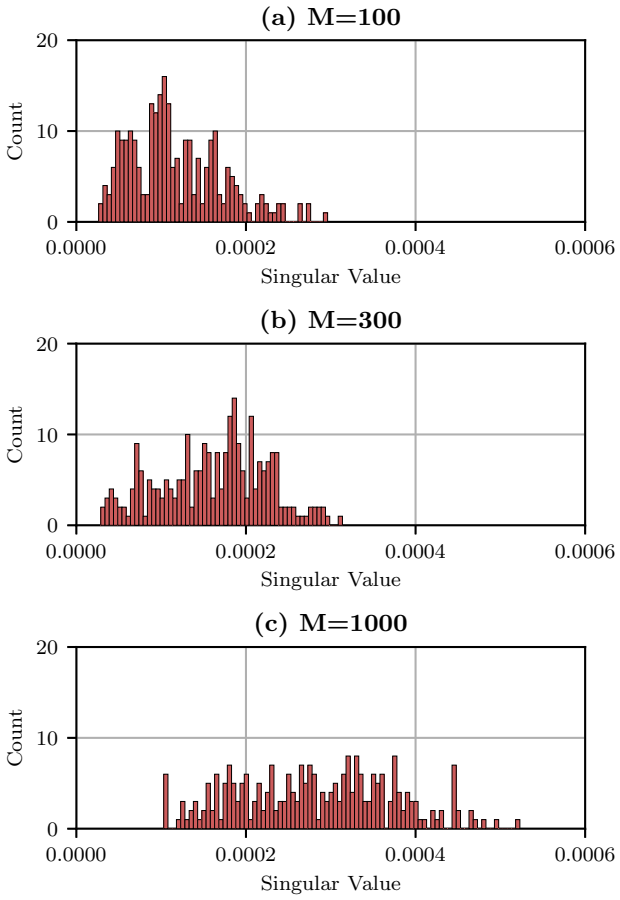

Fig. 4: Distribution of the singular values ($\sigma_{\min}$) varied over various M.

TABLE I: Minimum of $\sigma_{\min}$ for various methods over 100 trials

Method	median	min	max	std
Relaxed	6.4×10^{-5}	1.91×10^{-5}	1.61×10^{-4}	2.82×10^{-5}
Bruteforce	4.30×10^{-6}	2.07×10^{-6}	3.46×10^{-5}	4.10×10^{-6}
Rounded	3.59×10^{-7}	1.09×10^{-8}	4.12×10^{-6}	8.29×10^{-7}
Random	3.32×10^{-7}	7.70×10^{-10}	4.52×10^{-6}	8.29×10^{-7}

feasible solution. The brute force solution also outperforms the rounded solution which is not desirable but these statistics only describe the smallest $\sigma_{\min}$ over some angles but not the overall distribution of $\sigma_{\min}$ for all angles. To explore that, the distribution of $\sigma_{\min}$ over all angles was calculated and shown in Fig. 5 for a setup of $M = 15, K = 8$. In this distribution, we can see that although the minimum value of the rounded solution is smaller than brute force approach, the overall distribution of the $\sigma_{\min}$ seems to be higher than brute force and random.

D. Field Generation

The main goal of our optimization is to come up with a K magnet configuration that can generate various fields

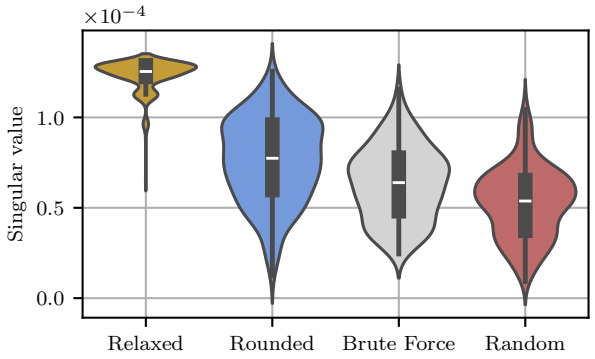

Fig. 5: Violin plot describing the singular value distributions of an 8-magnet configuration chosen from 15 randomly generated poses using various methods.

TABLE II: Maximum Fields and Forces achievable in each direction

Directions	x	y	z
B_{max} (mT)	17.4	16.8	26.5
F_{max} (mN)	4.87	4.08	2.81

and forces to control a microrobot remotely. To evaluate this capability, random, symmetric, and 2 optimal solutions with different M were compared for fields and forces in 50 random directions as shown in Fig. 6(a). The symmetric configuration is a manually designed configuration that one might intuitively come up with. A 5 mT field with zero force was used for the evaluation. Then for the chosen configuration of magnets, the inverse kinematics formulation (8) is used to find the K motor angles to give the desired field and force. The inverse kinematic equation is solved using the Broyden–Fletcher–Goldfarb–Shanno (BFGS) algorithm (SciPy). Finally, the field at the target location is derived for the calculated motor angles and the relative error is measured. A similar approach is used for the force error calculated for a 1 mN force, with a 1 mT field sampled in the same 50 randomly generated directions.

As shown in Fig. 6(b), (c) the optimal solution from a sample size of 100 performs slightly better than a symmetric design in terms of relative field and force errors. As expected, the solution for $M = 1000$ outperforms the rest by several orders of magnitude. This result suggests that an optimal magnet configuration will not be symmetric nor can be intuitively designed, and even an optimization with a low sample size of 100 can outperform such designs.

Another important aspect of a magnetic actuation system is the magnitude of the field and the forces produced. The maximum fields and forces the optimized system can generate are shown in Table II. The field produced in the z-direction is much higher than the other directions and this might be due to the layout of the system where the magnets are located under the target location.

Lastly, the workspace coverage of the generated magnetic fields is also crucial in the actuation system. This will ensure we can produce fields over a large workspace instead of being localized at the target location. To evaluate this, we

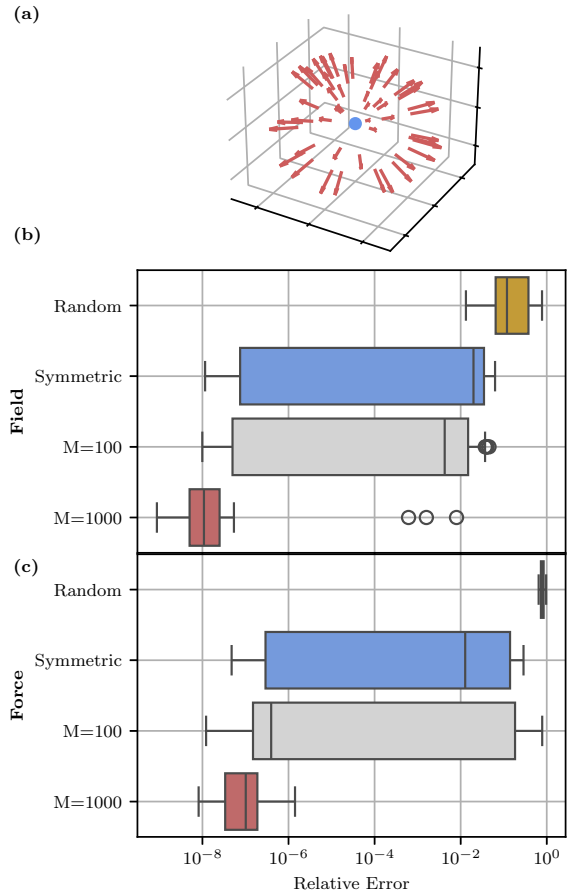

Fig. 6: Relative error in fields and forces for 50 random directions. (a) 50 sampled directions for forces and fields. (b) Field error for chosen configuration at 5 mT. (c) Force error for 1 mN force

visualized the magnetic field around the target location for a 12 mT field in 3 directions as shown in Fig. 7. For a field in the x or y direction, the field is fairly homogeneous around the target location in the xy plane giving us a workspace size of 10 cm by 10 cm. There is a noticeable change in field strength in the z-plane for a field in the x or y direction. This issue stems from our design, in which the distance to the magnet increases as you go further up as all the magnets are located below the target point. As fields and forces scale inversely with distance, this undesirable property affects the field homogeneity in the z-direction as the distance from the magnet changes.

V. Simulation

The effectiveness of the optimal design is also validated using a simulation environment constructed in Unity. The prototype design chosen was based on the optimal solution for $M = 1000$. The system's ability to produce the desired fields and forces was tested in two demos as shown in Fig. 8. The first demo included navigating a 3 mm target magnet through a simple maze which proved to be very accurate due to the system's ability to produce homogeneous fields in the x-y plane. The second demo included successfully

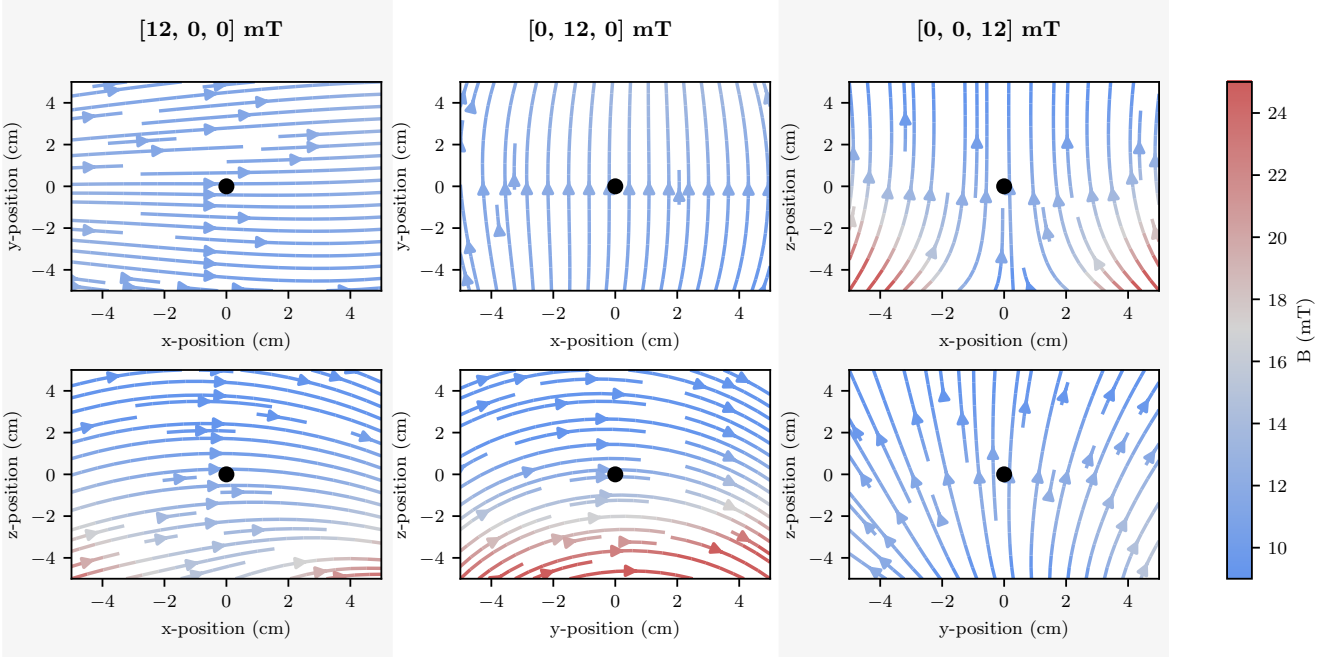

Fig. 7: Visualisation of the field around the target location for a 12 mT field generated in 3 directions around a 10 cm workspace

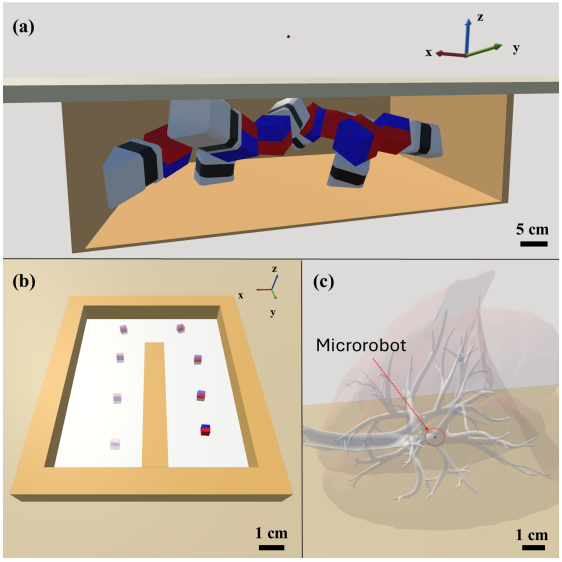

Fig. 8: (a) System setup in the simulation environment. (b) 3 mm cube navigated through a maze. (c) Microrobot being navigated through the lungs (using model from [15]).

navigating a spherical magnet through a bronchi model [15]. These simulated demonstrations are a promising indicator that the system can navigate microrobots in a 3D space.

VI. CONCLUSION AND DISCUSSION

In this paper, we developed a magnetic actuation platform using OMASTAR, a novel design optimization approach. Our magnetic actuation system fits under the operating table, allowing maximum workspace accessibility. OMASTAR is specifically designed to help avoid local minima in our objective function based on nonconvex magnetic field and force equations.

Long term, we hope to significantly improve this optimization scheme. Currently, $\boldsymbol{X}$ tends to be uniform along the columns, indicating symmetry in our approach which will be exploited in our future work to make the formulation more efficient. Although the fields produced are comparable to other actuation system designs, we would like to explore methods to increase the magnitude of the fields and forces generated. This can also be achieved by increasing the magnet size or quantity. The non-uniformity in the z-plane also needs to be addressed in future work by either changing the design or including other uniform sources of magnetic fields such as electromagnetic coils. Lastly, a physical prototype similar to the one in our simulation will be built for an experimental evaluation of the fields and forces, and application specific tests will be performed.

REFERENCES

[1] M. Sitti, H. Ceylan, W. Hu, J. Giltinan, M. Turan, S. Yim, and E. Diller, "Biomedical applications of untethered mobile milli/microrobots," 2015.
[2] P. E. Dupont, B. J. Nelson, M. Goldfarb, B. Hannaford, A. Menciassi, M. K. O'Malley, N. Simaan, P. Valdastri, and G. Z. Yang, "A decade retrospective of medical robotics research from 2010 to 2020," 2021.
[3] U. Bozuyuk, P. Wrede, E. Yildiz, and M. Sitti, "Roadmap for clinical translation of mobile microrobotics," 2024.
[4] H. Ceylan, I. C. Yasa, U. Kilic, W. Hu, and M. Sitti, "Translational prospects of untethered medical microrobots," 2019.
[5] B. Wang, K. Kostarelos, B. J. Nelson, and L. Zhang, "Trends in micro-/nanorobotics: Materials development, actuation, localization, and system integration for biomedical applications," 2021.
[6] A. Schonewille, C. He, C. Forbrigger, N. Wu, J. Drake, T. Looi, and E. Diller, "Electromagnets under the table: An unobtrusive magnetic navigation system for microsurgery," *IEEE Transactions on Medical Robotics and Bionics*, vol. 6, pp. 980–991, 8 2024.

[7] W. Lee, E. Jung, N. Kim, D. Lee, S. Kim, Y. Lee, and G. Jang, "Robotically adjustable magnetic navigation system for medical magnetic milli/microrobots," *IEEE/ASME Transactions on Mechatronics*, 2024.
[8] B. E. Kratochvil, M. P. Kummer, S. Erni, R. Borer, D. R. Frutiger, S. Schürle, and B. J. Nelson, "Minimag: A hemispherical electromagnetic system for 5-dof wireless micromanipulation," in *Springer Tracts in Advanced Robotics*, vol. 79, 2014.
[9] D. Son, X. Dong, and M. Sitti, "A simultaneous calibration method for magnetic robot localization and actuation systems," *IEEE Transactions on Robotics*, vol. 35, 2019.
[10] S. Erni, S. Schürle, A. Fakhraee, B. E. Kratochvil, and B. J. Nelson, "Comparison, optimization, and limitations of magnetic manipulation systems," *Journal of Micro-Bio Robotics*, vol. 8, 2013.
[11] F. Carpi and C. Pappone, "Stereotaxis niobe® magnetic navigation system for endocardial catheter ablation and gastrointestinal capsule endoscopy," 2009.
[12] G. Pittiglio, J. H. Chandler, M. Richter, V. K. Venkiteswaran, S. Misra, and P. Valdastri, "Dual-arm control for enhanced magnetic manipulation," in *IEEE International Conference on Intelligent Robots and Systems*, 2020.
[13] J. Hwang, J. young Kim, and H. Choi, "A review of magnetic actuation systems and magnetically actuated guidewire- and catheter-based microrobots for vascular interventions," 2020.
[14] P. Ryan and E. Diller, "Magnetic actuation for full dexterity microrobotic control using rotating permanent magnets," *IEEE Transactions on Robotics*, vol. 33, pp. 1398–1409, 12 2017.
[15] A. Sieben and M. R. Jongbloed, "Normal Lungs, CC BY-NC-SA."
[16] P. Kaveti, M. Giamou, H. Singh, and D. M. Rosen, "Oasis: Optimal arrangements for sensing in slam," 9 2023.
[17] M. W. Spong, S. Hutchinson, and M. Vidyasagar, "Robot modeling and control," 2006.
[18] K. Chaloner and I. Verdinelli, "Bayesian experimental design: A review," *Statistical Science*, vol. 10, 8 1995.
[19] R. Hemmecke, M. Köppe, J. Lee, and R. Weismantel, *Nonlinear Integer Programming*, p. 561–618. Springer Berlin Heidelberg, Nov. 2009.
[20] S. Boyd and L. Vandenberghe, *Convex optimization*. Cambridge university press, 2004.
[21] K. J. Doherty, D. M. Rosen, and J. J. Leonard, "Spectral measurement sparsification for pose-graph slam," in *2022 IEEE/RSJ International Conference on Intelligent Robots and Systems (IROS)*, pp. 01–08, IEEE, 10 2022.
[22] A. J. Petruska and B. J. Nelson, "Minimum bounds on the number of electromagnets required for remote magnetic manipulation," *IEEE Transactions on Robotics*, vol. 31, 2015.